Plasmonics
https://doi.org/10.1007/s11468-024-02401-6

RESEARCH

Versatile Terahertz Metamaterial Sensor for Biomedical Applications

Mahmoud Maree E. Tammam[1] · Mohamed Farhat O. Hameed[2] · Essam M. A. Elkaramany[1] · Tamer A. Ali[1,3] · S. S. A. Obayya[4]

Received: 9 May 2024 / Accepted: 17 June 2024

Abstract
In this work, we propose a THz metamaterial for biomedical applications. The full vectorial finite element method is used to design and analyze the reported biosensor. The proposed sensor is based on increasing the confinement of the electric and magnetic fields at the analyte layer at the resonance frequency. Hence, any slight variation of the optical properties of the analyte sample (typically the refractive index) can be detected. We demonstrate the potential of using the reported sensor for hemoglobin (Hb) concentration and early cancer detection. The geometrical parameters are studied to maximize the sensor sensitivity of the symmetric and asymmetric designs. An absorptivity of 0.98 is achieved at 1.1 THz, which depends on the analyte sample refractive index**.** High sensor sensitivity of 1.08 GHz/g/dL is obtained with high Q-factor of 13.2 and FWHM (full width at half maximum) of 140 GHz through hemoglobin (Hb) concentration change from 5 g/dL to 20 g/dL. Further, an average sensitivity of 556.325 GHz/RIU is realized for cancer early detection for basal cell, breast cell, Jurkat cell and Cervical cell. Therefore, the proposed design is a good candidate for biomedical applications.

Keywords Metamaterial · Hemoglobin sensing · Cancer detection · FEM · Biosensor

Introduction

Metamaterials [1] are artificial structures with unique characteristics that can be created by smaller elements in size than the external stimulus. Metamaterials consist of two layers of metal separated by dielectric layer. The resultant permittivity ε(ω) and permeability μ(ω) can't be achieved by conventional materials [2] which depend on the geometrical properties of metallic patch shape and mutual distance between them [3, 4]. Metamaterials, in particular, have become increasingly popular in recent years for a variety of purposes; such as negative refraction [5], polarization rotation [6], source imaging [7], energy harvesting [8], sensor technology [9], perfect absorption [10], super lenses [11], and antennas [12].

Metamaterials have become one of the most promising materials in attempt to achieve perfect absorption. The use of metamaterial absorbers has also been explored for biomonitoring purposes in the terahertz domain. High-flexible absorber has been fabricated with absorptivity of 0.97 at f = 1.6 THz [13]. Areed et al. have proposed a near-perfect metamaterial absorbance with an absorbency of 0.97 across the visible wavelength range [14]. Metamaterial right/left-handed transmission line has been studied for sensing applications [15]. Lee et al. have also introduced metamaterial sensor based on split ring resonators [16]. A nearly zero permittivity metamaterial biosensor with enhanced sensitivity has proposed [17]. Another design of nearly perfect metamaterial absorber was suggested and analyzed for terahertz sensing applications with absorptivity of 0.99 at f = 2.249 THz [18]. A highly sensitive sensor

✉ Mohamed Farhat O. Hameed
engmfarhat@mans.edu.eg

✉ S. S. A. Obayya
sobbaya@zewailcity.edu.eg

[1] Mathematics and Engineering Physics Department, Faculty of Engineering, Cairo University, Giza 12613, Egypt

[2] Mathematics and Engineering Physics Department, Faculty of Engineering, University of Mansoura, Mansoura 35516, Egypt

[3] Communications and Information Engineering Program, University of Science and Technology, Zewail City of Science, Technology and Innovation, October Gardens, Giza 12578, Egypt

[4] Centre for Photonics and Smart Materials, Zewail City of Science, Technology and Innovation, October Gardens, Giza 12578, Egypt

Published online: 29 August 2024

for virus detection was presented using terahertz nano-gap metamaterials [19]. Further, microbial detection using a metamaterial absorption absorber was introduced in [20]. A metamaterial sensor was designed for non-destructive evaluation of dielectric substrates [21]. Dual band metamaterial cancer cell sensor with a maximum sensitivity of 196.5 GHz/RIU has been proposed [22]. Additionally, a hyperbolic metamaterial sensor with a maximum sensitivity of 500 nm/RIU has been introduced for the detection of cancer cells [23].

Haemoglobin (Hb) is located in red blood cells and is responsible for O_2 transport in the circulatory system. Polycythemia is diagnosed when the Hb level in the blood is greater than the maximum limits. However, Anaemia is detected when the Hb level is less than the minimal limit. There is a need for immediate detection and easy technique to measure the (Hb) level in the blood. In this context, different types of electrical, and optical sensors were proposed for the detection of Hb concentrations. A dual-core photonic crystal fiber (PCF) sensor has been introduced for Hb concentration monitoring in the blood [24]. A two-dimensional photonic crystal-based for hemoglobin biosensor with a sensitivity and quality factor of 272.43 nm/RIU and 3000, respectively, have been proposed [25]. Further, highly sensitive one-dimensional photonic crystal (1D PhC) sensor for hemoglobin (Hb) concentration monitoring is proposed and analysed [26]. A highly sensitive PCF hemoglobin sensor was also numerically simulated and studied with sensitivity of 2080 RIU − 1 with a resolution of $4.80 \times 10 - 6$ RIU at a hemoglobin refractive index of 1.38 [27]. Moreover, El-Khozondar et al. [28] have suggested plasma blood sensor with sensitivity of 51.4 nm/RIU at concentration range of (0–50 g/L). Additionally, an optical sensor system for hemoglobin measurement was implemented in [29]. A multi-wavelength light absorption device to measure hemoglobin concentration was reported in [30]. However, the design of metamaterial sensor for Hb concentration is very limited in the literature.

According to the International Agency for Research on Cancer (IARC), cancer is the second leading cause of death worldwide. Cancer is a malignant genetic disorder that can be produced by a malfunction in the division of cells in the human body. Nowadays, a lot of research is conducted to explore the possibility of detecting tumors in the human body using microwave signals. The primary benefit of microwave imaging is its nonionizing nature and, as a rule of thumb, its cost-effectiveness. Cancer detection must be conducted at the cellular level in the early stages of cancer in order to enable the patient to receive early detection and treatment. In recent years, a number of research papers has been published using metamaterial biosensor for the cancer early detection. In this context, Cong and Singh [31] have presented a metamaterial absorber sensor with sensitivity of 163 GHz/RIU, and Q-factor of 7.036. Additionally, metamaterial terahertz biosensor was proposed for early-stage detection of cervical cancer tissue using with two resonant absorption frequencies [32]. Zhang et al. [33] introduced MM-based THz biosensor to analyze the apoptosis of dried cancer cells. Han et al. [34] employed MM-based THz biosensor with theoretical sensitivity of the MMs sensor is about 287 GHz/RIU. Additionally, Manikandan et al. [35] have suggested dual-band metamaterial cancer cell sensor with sensitivity of 196.5 GHz/RIU, and Q- factor of 165. Moreover a graphene-based metamaterial sensor has been implemented for different types of cancer cells with a sensitivity of 207.14 GHz/RIU, a quality factor of 13 [36].

In this paper, THz asymmetric metamaterial design is proposed and analyzed for biomedical applications including Hb concentration detection and cancer cell detection. The geometrical parameters are studied to maximize the sensor sensitivity. The simulation results are obtained using full vectorial finite element method. It is found that high sensor sensitivity of 1.08 GHz/g/dL is achieved through hemoglobin (Hb) concentration change from 5 g/dL to 20 g/dL. The potential of using the reported design for cancer early detection is also demonstrated with an average sensitivity of 556.325 GHz/RIU. The reported biosensor has a higher sensitivity than those suggested in [31, 33, 35, 36] for cancer early detection.

Design and Fabrication Considerations

Figure 1 shows the suggested design of asymmetric metamaterial biosensor. The proposed structure is composed of two layers of gold, which are separated by a dielectric material. The top layer of thickness h_1 has an array of metallic patches. Each patch consists of a rectangle resonator with line width s, and gap G as shown in Fig. 1(a). A single bottom layer of gold is used with a thickness of h_1 as a lossy media with conductivity independent of frequency $\sigma = 4.09 \times 10^7$ S/m [13]. The dielectric medium is polyimide with a thickness $h_2 = 8.5$ μm and refractive index $n = 2.88 - 0.09j$ [37]. In the suggeted design, the parameters *a* and *d* are used to control the shift of the central gap in x and y directions, respectively.

Metamaterials are engineered materials that possess distinct properties, with a permittivity (ε) that is smaller than the free space permittivity (ε_0), and a permeability < free space permeability (μ_0). In this study, the effective

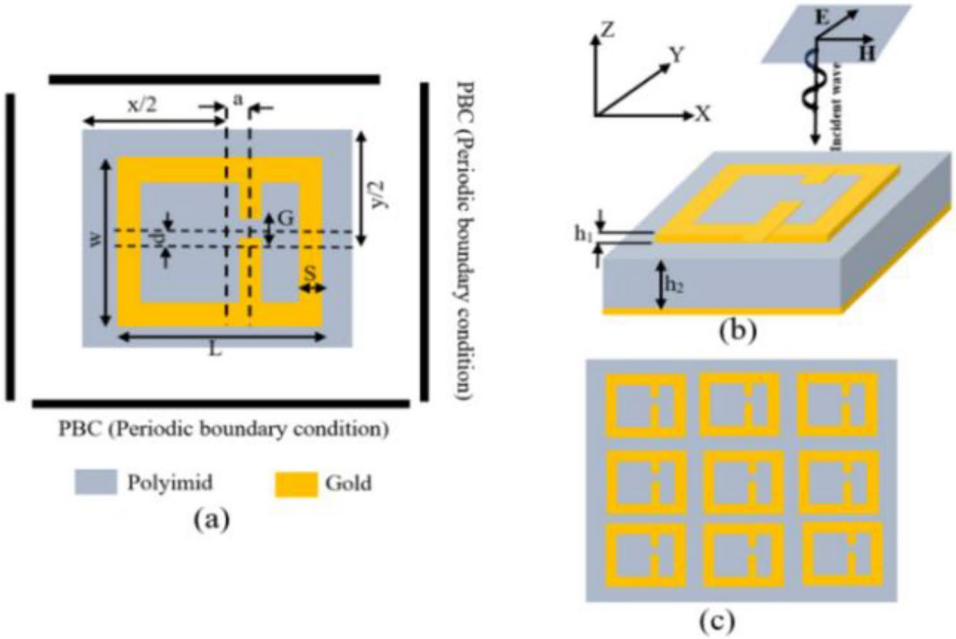

Fig. 1 **a** Two- and **b** three-dimension schematic diagrams of the unit cell of the reported metamaterial biosensor and **c** the proposed patch array

permittivity (ε_{eff}), and effective permeability (μ_{eff}) are obtained through the S-parameters as given by [38]:

$$\varepsilon_{eff} = 1 + \frac{2j}{K_o h_2}\left(\frac{1 - S_{11}}{1 + S_{11}}\right) \tag{1}$$

$$\mu_{eff} = 1 + \frac{2j}{K_o h_2}\left(\frac{1 + S_{11}}{1 - S_{11}}\right) \tag{2}$$

where K_o is the free space wave number, h_2 is the substrate thickness, and S_{11} is the reflection coefficient. The frequency dependent relative permittivity ε_r and relative permeability μ_r of the reported design are shown in Fig. 2. It may be seen that both ε_r and μ_r have negative real parts through the frequency range from 1.15 THz to 1.28 THz, hence the proposed metamaterial has double negative feature. Therefore, it is expected that a resonance can occur with maximum absorption in this region.

The impedance (Z) of the ideal absorber should be closely matched to the free space impedance in order to reduce the reflection from the surface [39].

$$Z = \pm\sqrt{\frac{(1 + S_{11}(\omega))^2 - S_{21}^2(\omega)}{(1 - S_{11}(\omega))^2 - S_{21}^2(\omega)}} \tag{3}$$

where S_{21} is the transmission coefficient, and ω is the angular frequency. Figure 3 shows the real and imaginary parts of the relative impedance of the proposed design. It may be seen that at the resonance frequency 1.25 THz, the real part and imaginary part of relative impedance are close to 1, and zero, respectively. Consequently, at the resonance frequency, the incident light will be transmitted and absorbed by the metamaterial design.

Using equivalent circuit theory, it is possible to understand the change in the resonance peaks as follows [40]:

$$f = \frac{1}{2\pi\sqrt{L_{eq}C_{eq}}} \tag{4}$$

where f is the resonance frequency, and L_{eq}, and C_{eq} are the equivalent inductance and capacitance of the sensor. It is possible to infer that the frequency of resonance corresponds to the inverse square root of the corresponding capacitance, which is increased by the increase in the analyte Refractive Index (RI). Therefore, the resonance frequency is red shifted by increasing the analyte RI, which may be also explained by the first order electromagnetic perturbation theory [41]. Additionally, the positive charges are concentrated at the bottom metallic layer, acting as a weak electric dipole, while the negative charges are focused at the top metallic strip [42].

Symmetric structure is first studied with a = d = 0, as shown in the inset of Fig. 4. The initial design parameters are L = W = 38 μm, c = 12 μm, s = 3 μmm, G = 2 μm, x = y = 50 μm. The simulation of the symmetrical sensor design is based on the full vectorial finite element approach [43] utilizing the COMSOL Multiphysics Software Package (comsol.com) [44]. Using a non-uniform mesh, the 3D computational unit cell is discretized into 367,299 tetrahedral domain elements, 47,706 boundary elements, and 1864 edge elements with a minimum element size of 7.2 nm. Moreover, boundary condition of perfect electric conductor is applied

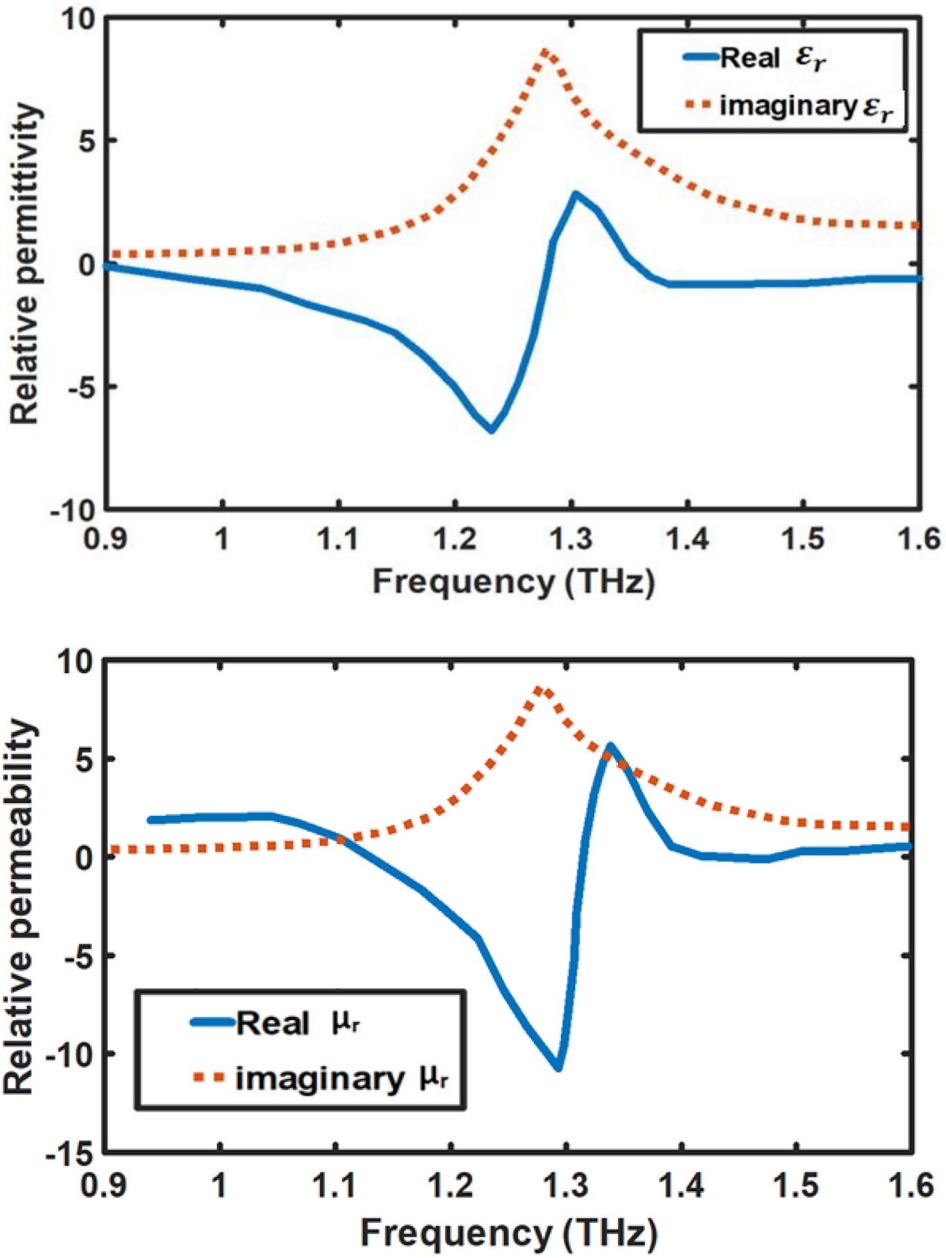

Fig. 2 Frequency dependent **a** effective permittivity, and **b** effective permeability of the reported metamaterial absorber

in y-direction while perfect magnetic conductor is used in x-direction. This is equivalent to applying Floquet periodic boundary condition (FPBC) in x- and y-directions to reduce the computational domain. Further, the ground plane and top metal patches are subjected to impedance boundary and transition boundary conditions, respectively.

A plane wave is also excited using a single port with a power 1W with a normal incidence. The electric field also has unity in the y-direction. The light absorption A through the suggested design can be calculated as follows

$$A = 1 - S_{11}^2 - S_{21}^2 \tag{5}$$

Because of the bottom gold layer, which behaves as an optical mirror in the used frequency range, $S_{21} = 0$. Figure 4 shows the absorption spectra where the resonance occurs at f = 1.25 THz, which is compatible with that presented in [13]. At the resonance frequency, the field is confined in the gap region as shown in the inset of Fig. 4. It is expected that the resonance frequency will be sensitive to the surrounding variation in the refractive index of the medium.

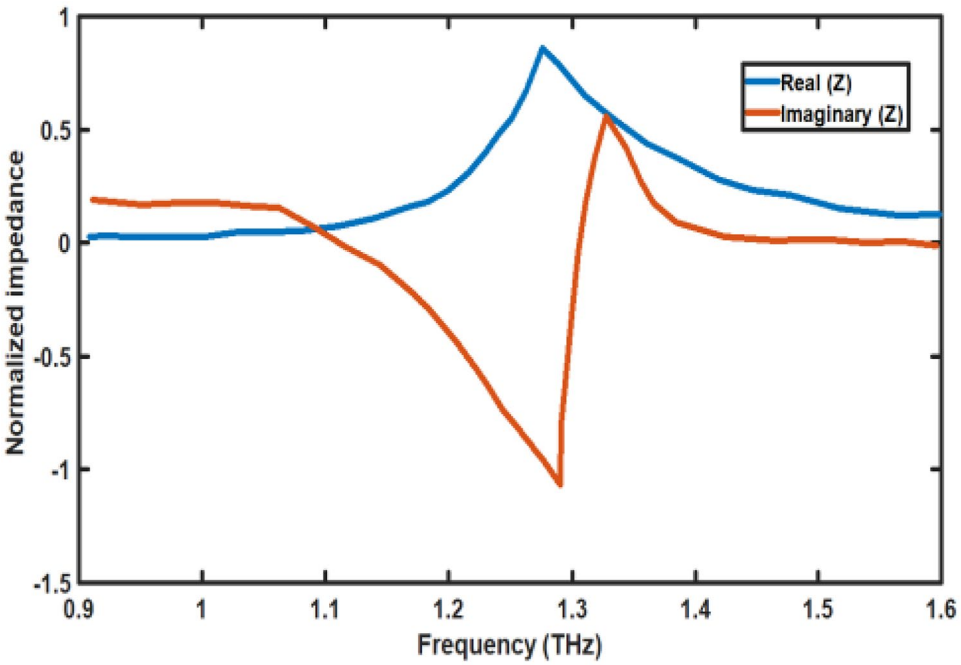

Fig. 3 The real part and imaginary part of the relative impedance for the resonance peak

To demonstrate the accuracy of our model, a comparison study is conducted using the simulated and experimental absorption spectra of the metamaterial absorber reported in [7]. It may be seen from Fig. 5 that a good agreement is achieved between the simulation results. Additionally, the simulated resonance frequency is compatible with the measured resonance frequency [7] which guarantees the accuracy of our model.

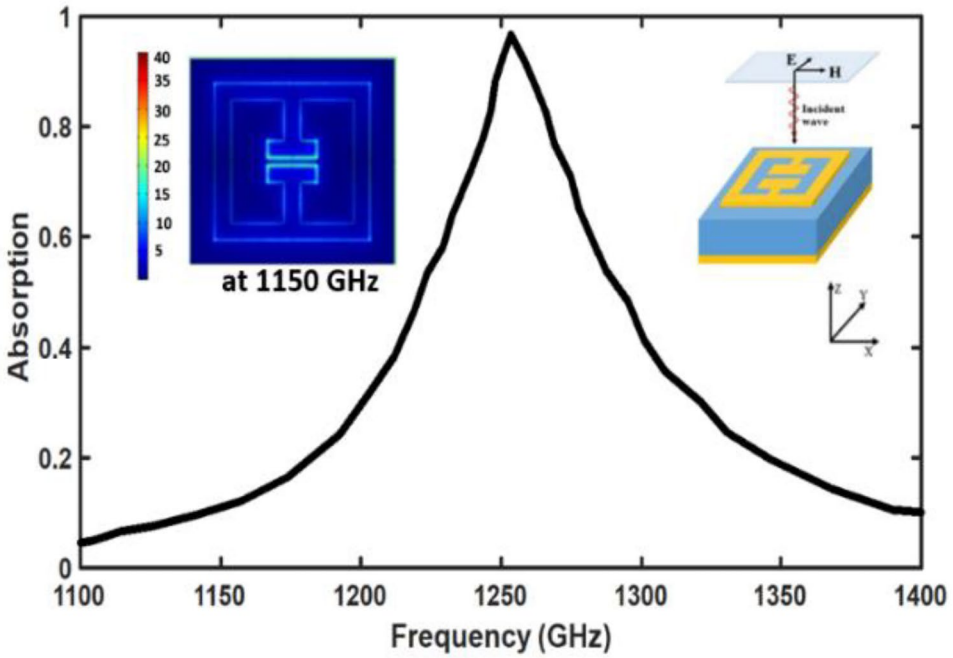

Fig. 4 Frequency dependent absorption of the symmetric metamaterial sensor

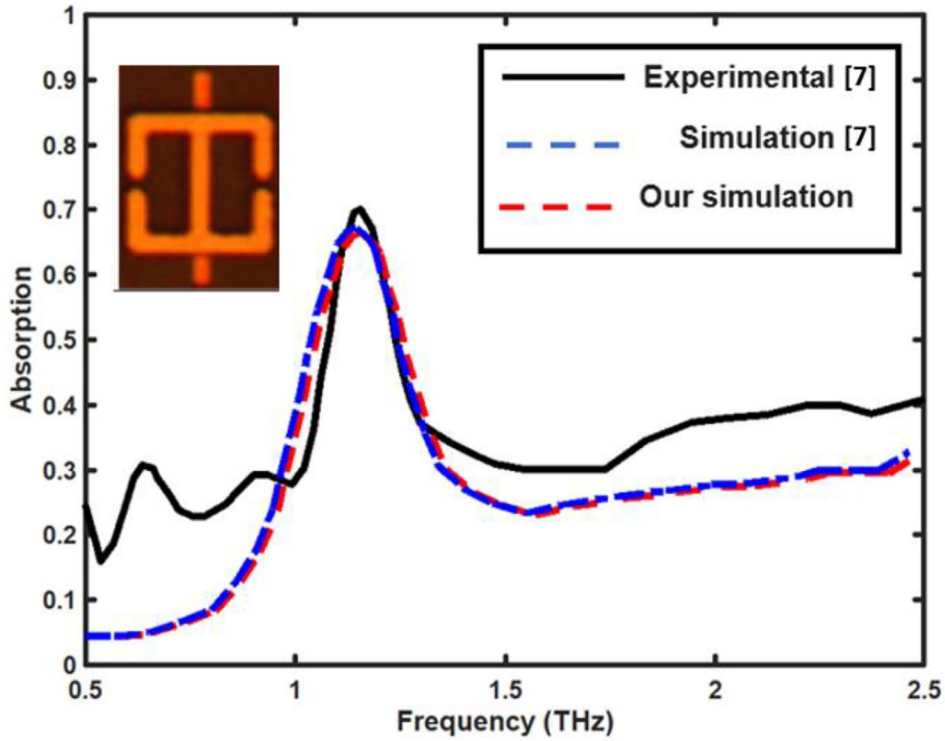

Fig. 5 Comparison between the measured and calculated frequency dependent absorptions of the metamaterial absorber reported in [7] and our calculations

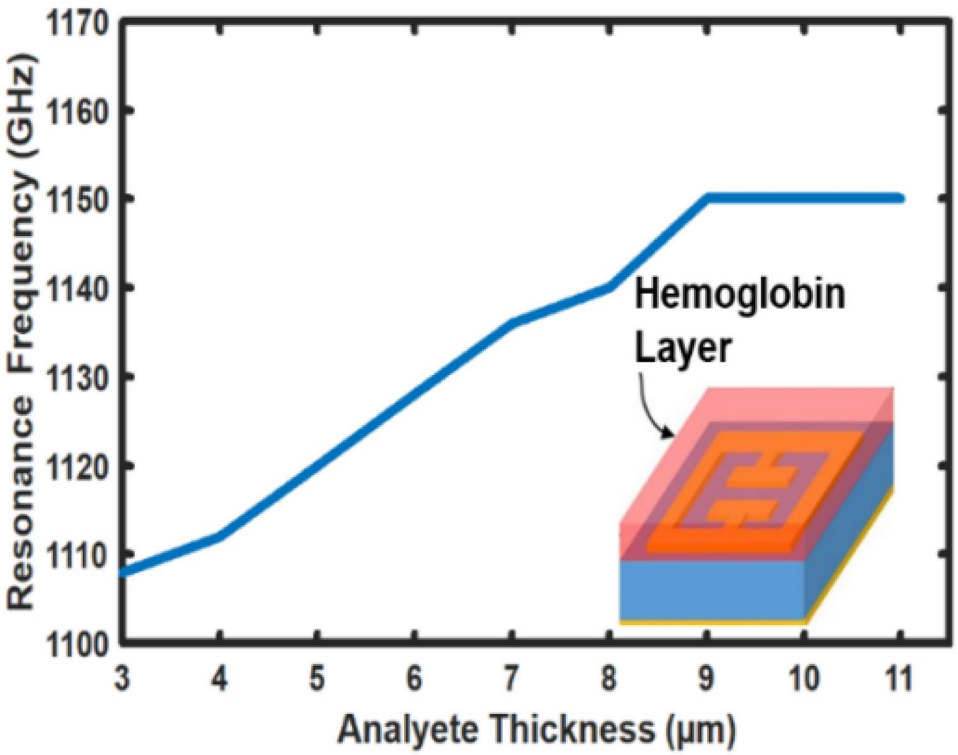

Fig. 6 Dependence of the resonance frequency on the analyte thickness

Hemoglobin Concentration Measurement Biosensor

To test the potential of using the studied design as a biosensor, a hemoglobin sample is placed over the metamaterial as shown in the inset of Fig. 6. The wavelength dependent refractive index n_{Hb} of the hemoglobin depends on its concentration C_{Hb} as given by:

$$n_{Hb}\left(\lambda, C_{Hb}\right) = n_{H_2o}(\lambda)[\beta(\lambda)C_{Hb} + 1] \tag{6}$$

where $n_{H_2o}(\lambda)$ is the wavelength-dependent water refractive index, β(λ) is a wavelength-dependent increase in the water's refractive index in (g/dL) [45], and C_{Hb} is the concentration of the hemoglobin in g/dL [46]. Figure 7 shows the effect of analyte thickness on resonance frequency. It is evident that that the resonance frequency does not change significantly beyond 9 μm analyte thickness which will be used for the subsequent simulation.

Figure 5 shows the frequency dependence of the absorption curve on different hemoglobin concentrations. It may be seen that the resonance frequency slightly increases by increasing the hemoglobin concentration. Therefore, C_{Hb} change can be detected using the resonance shift and the sensor sensitivity is calculated as follows [18]:

$$\text{Sensitivity} = \frac{\Delta\ Resonance\ frequency}{\Delta\ C_{Hb}} \tag{7}$$

The quality factor (Q) of the reported sensor is also calculated [18]:

$$Q = \frac{f_{res}}{FWHM} \tag{8}$$

where f_{res} is the resonance frequency and FWHM is the full width at half maximum of the absorption peak.

It is aimed to maximize the sensor sensitivity; therefore, parametric sweep study is performed on the different geometrical parameters. It should be noticed that the geometrical parameters alter the equivalent circuit's values for inductance and capacitance, which affects the resonance frequency. Figure 8(a) shows the effect of the line width *s* on the biosensor sensitivity. However, the other geometrical parameters are fixed at their initial values. As shown in Fig. (8-a), the biosensor sensitivity has a maximum value at line width 3.8 μm where the electric field is more confined in the gap region (as shown in the inset field plot of the E_x-component of X-polarized mode). Figure (8-b) illustrates the dependence of the sensor sensitivity on the gap size G at s = 3.8 μm. It may be seen that the optimum value for the gap is 2.75 μm where the biosensor sensitivity is maximum of 0.866 GHz/g/dL. Figure (8-c) shows the biosensor sensitivity as a function of the capacitor length at s = 3.8 μm and G = 2.75 μm where the electric field is more confined between gap at c = 3.8 μm. Changing the gap side length, gap, and line width affects the equivalent capacitance and the equivalent inductance, which change the resonance frequency.

The optimum geometric parameters for the symmetric structure are s = 3.8 μm, G = 2.75 μm, c = 4 μm and plyimide thickness of 8.5 μm for optimum sensitivity. These geometrical parameters are chosen to improve the sensitivity of

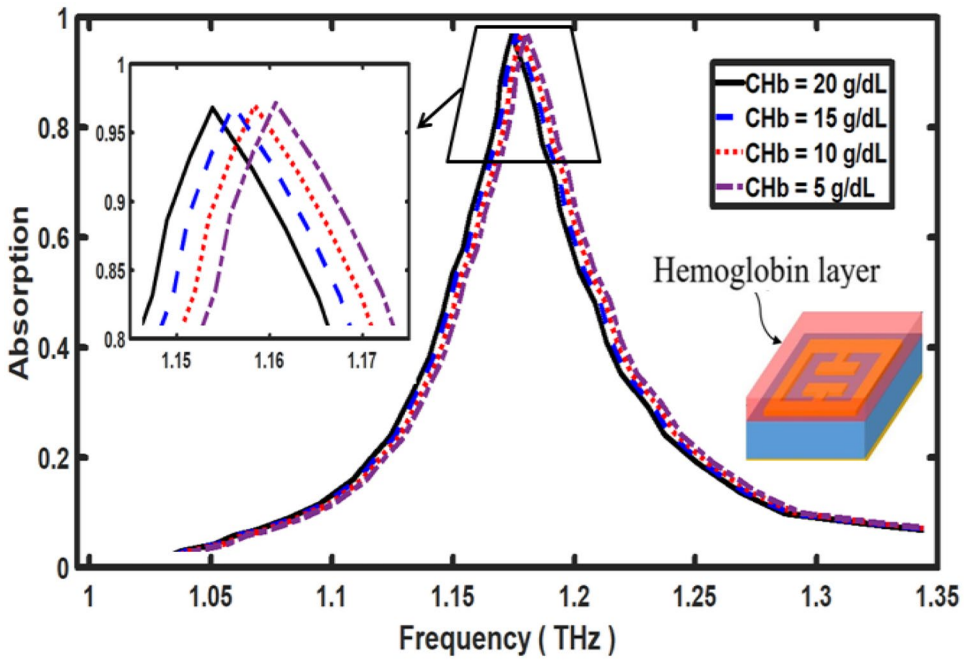

Fig. 7 Variation of the absorption of the metamaterial biosensor with the frequency at different hemoglobin concentrations

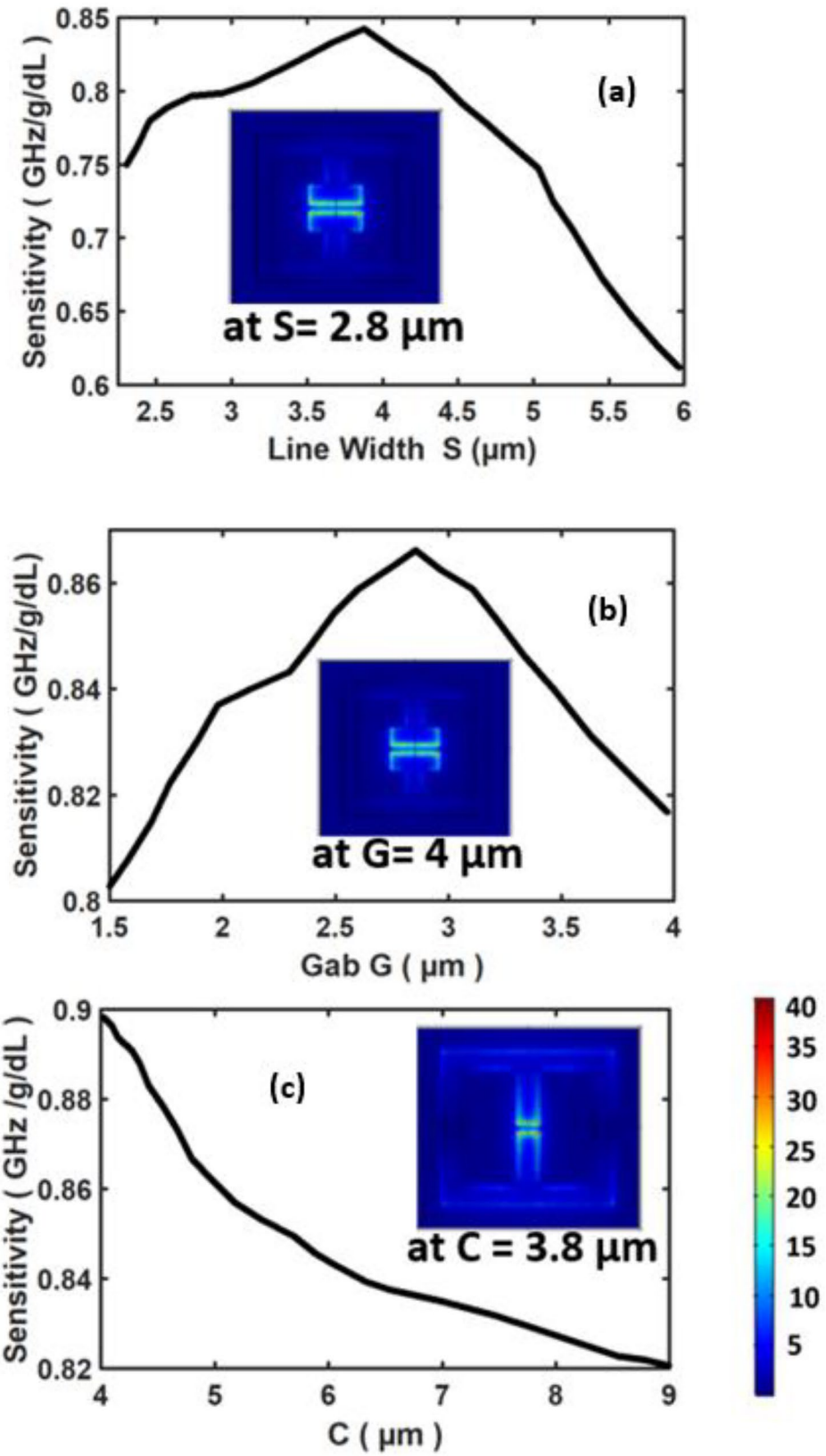

Fig. 8 The dependence of the biosensor sensitivity on the geometrical parameters; **a** line width s, **b** gap G and **c** capacitive line length C

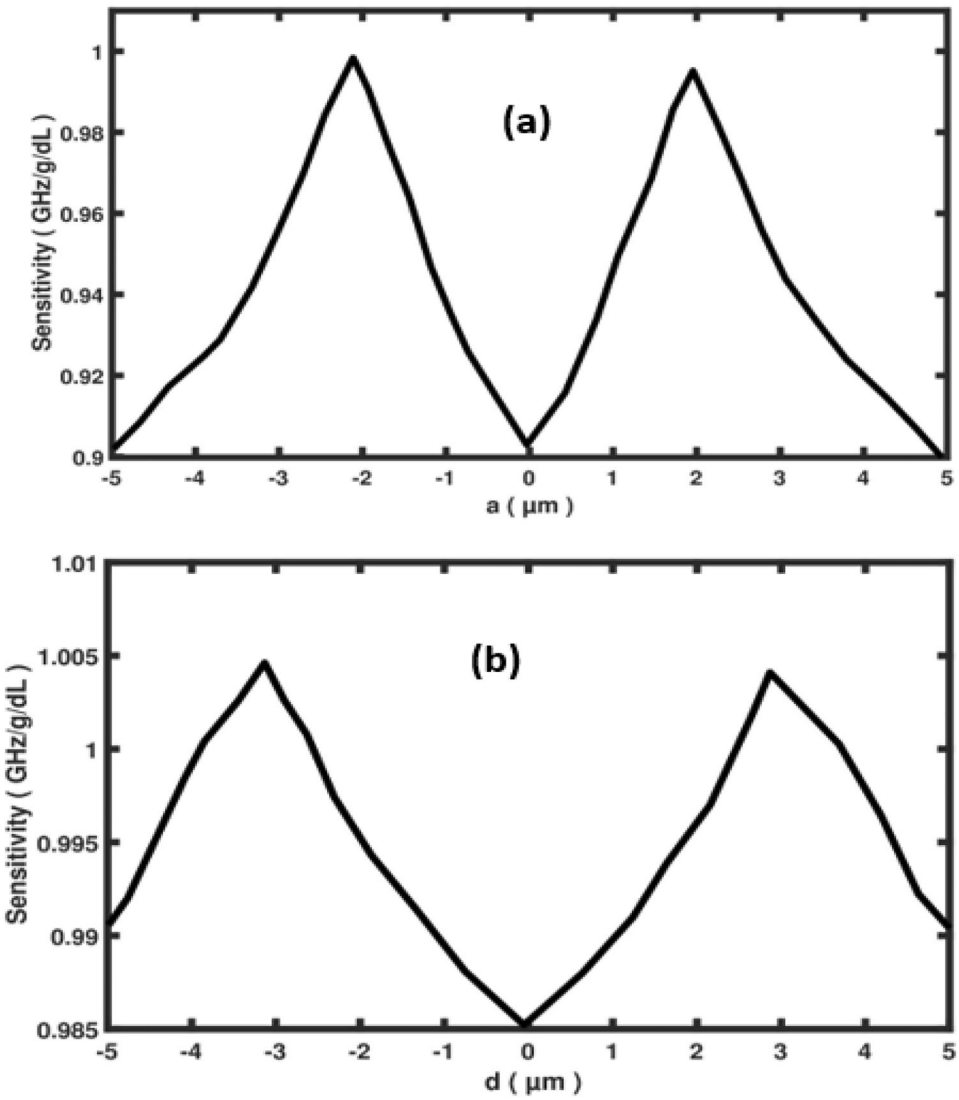

Fig. 9 The effect of the asymmetric parameters **a** a, and **b** d at a = 2 μm on the biosensor sensitivity

the sensor. To increase the biosensor sensitivity, asymmetric structure is used as revealed from Fig. 1(a). Figure 9(a) illustrates the effect of the shift distance (a) while the impact of d at $a = 2$ μm is illustrated in Fig. 9(b). It is evident form Fig. 9 that the asymmetric structure increases the biosensor sensitivity from 0.9 GHz/g/dL at a = d = 0 to 1.01 GHz/gm/dL at a = 2 μm and to 1.08 GHz/gm/dL at d = 3 μm. Figure 10 shows the absorption of the reported asymmetric metamaterial biosensor at different Hb concentrations. The resonance frequency is varied from 1115 to 1095 GHz by increasing the Hb concentration from 5 g/dL to 20 g/dL. Additionally, high quality factor of 74.333 is achieved at Hb concentration of 5 g/dL.

The linear performance of the reported biosensor is analyzed within the given frequency range. The variation of the resonance frequency with the Hb concentration is shown in Fig. 11. It may be seen that a linear fitting can be obtained for the suggested biosensor as given by

$$\begin{aligned} &\textit{resonance frequency}\ (GHz) \\ &= -1.32 \times 10^{-3} \times C_{Hb}(THz) + 1.121\ (THz) \end{aligned} \tag{9}$$

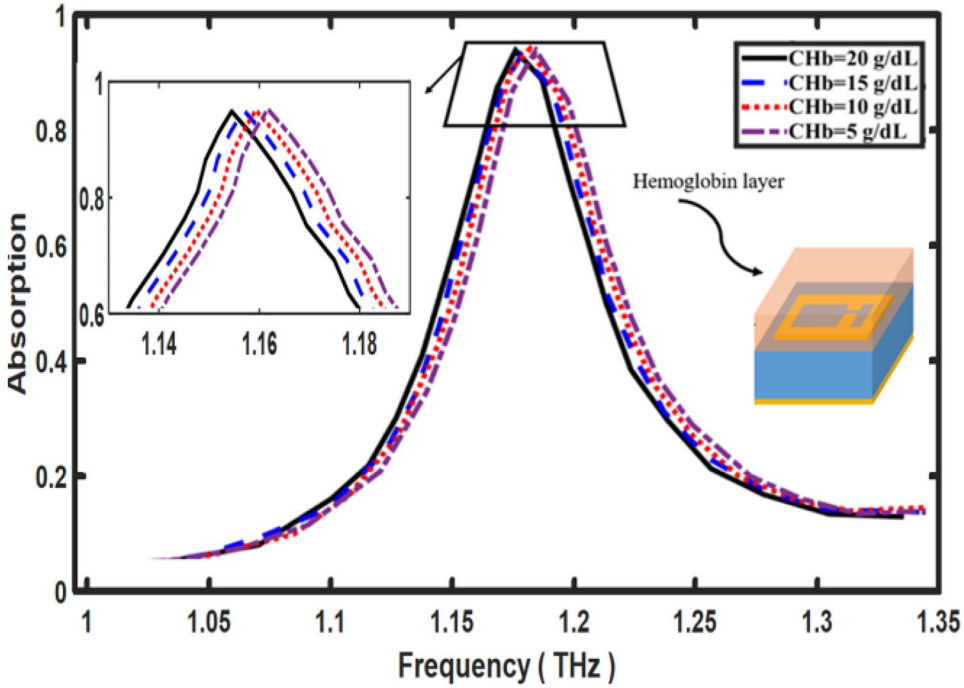

Fig. 10 Frequency dependent absorption of the metamaterial absorber bio-sensor at different concentrations using asymmetric metamaterial biosensor

The fitting line has R-square value of 0.9986 with high linear performance. A comparison is also made as revealed from Table 1 to show the merits of the proposed metamaterial biosensor. It may be seen that our suggested sensor has a higher linear sensitivity than the early presented sensors in the literature.

Cancer Early Detection Biosensor

The reported design is also investigated for early cancer detection including basal, breast, cervical, and jurkat cells. The normal and cancerous studied cells have refractive indices presented in Table 1 [47]. Figure 12 shows the

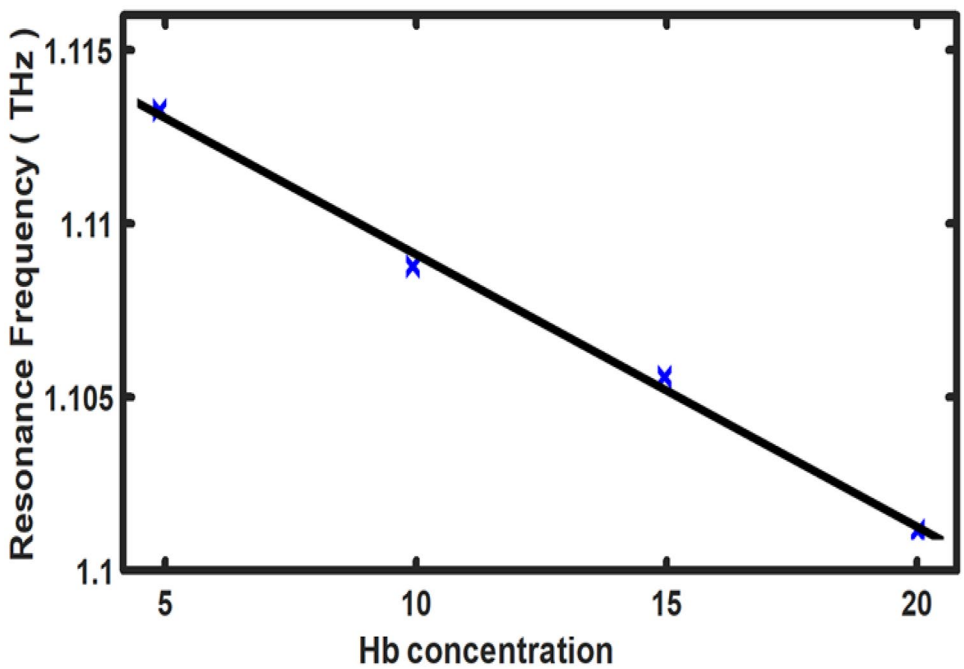

Fig. 11 Variation of the resonance frequency with the Hb concentration. Also, the linear fitting is demonstrated by black line

Table 1 The sensor performance of the reported biosensor for basal, breast, cervical, and jurkat cells

Cell name	State	Resonance frequency (GHz)	Sensitivity (GHz/RIU)	Quality Factor
Cervical	Cancer n = 1.392	1266	583.3	42.2
	Normal n = 1.368	1280		
Basal cell	Cancer n = 1.38	1272	500	44
	Normal n = 1.36	1282		
Breast cell	Cancer n = 1.399	1260	571	44
	Normal n = 1.385	1268		
Jurkat	Cancer n = 1.39	1270	571	43
	Normal n = 1.376	1278		

absorption spectra using normal and cancerous cells where the resonance frequencies are summarized in Table 2. The sensor sensitivity is calculated using the resonance frequency shift as given by

$$\text{sensitivity} = \frac{\Delta\ Resonance\ frequency}{\Delta\ n}\ GHz/RIU \tag{10}$$

The sensor sensitivity and quality factor of each case are calculated and introduced in Table 1. It may be seen that the suggested biosensor achieves an average sensitivity of 556.325 GHz/RIU with simple design. The performance of the reported biosensor is shown in Table 2 compared to previous designs. It may be seen that the current sensor sensitivity is higher than the other metamaterial structures with simple design. Although, the metamaterial sensor reported by Zhengzheng [52] has higher sensitivity than our design, however, it has complex design which will be challenge for fabrication. Therefore, the reported metamaterial sensor has high sensitivity with simple design for fabrication.

The proposed sensor can be manufactured using state-of-the-art technology. First, the background gold layer with a thickness of up to 200 nm can be deposited onto a GaAs or silicon wafer through e-beam evaporation [41]. Next, the liquid polyimide will be deposited onto the top surface of the gold layer by spin- coating. Then, it will be heated to 110 °C for 6 min on a hot plate [53]. The next step is to cure it for 5 h in a 275 °C oven in a nitrogen medium to form dielectric layers with thicknesses of 0.5 µm to 8 µm. An additional layer of gold is formed on the upper surface of polyimide through e-beam evaporation. In addition, photoresist layers can deposited on the upper dielectric layers with spin

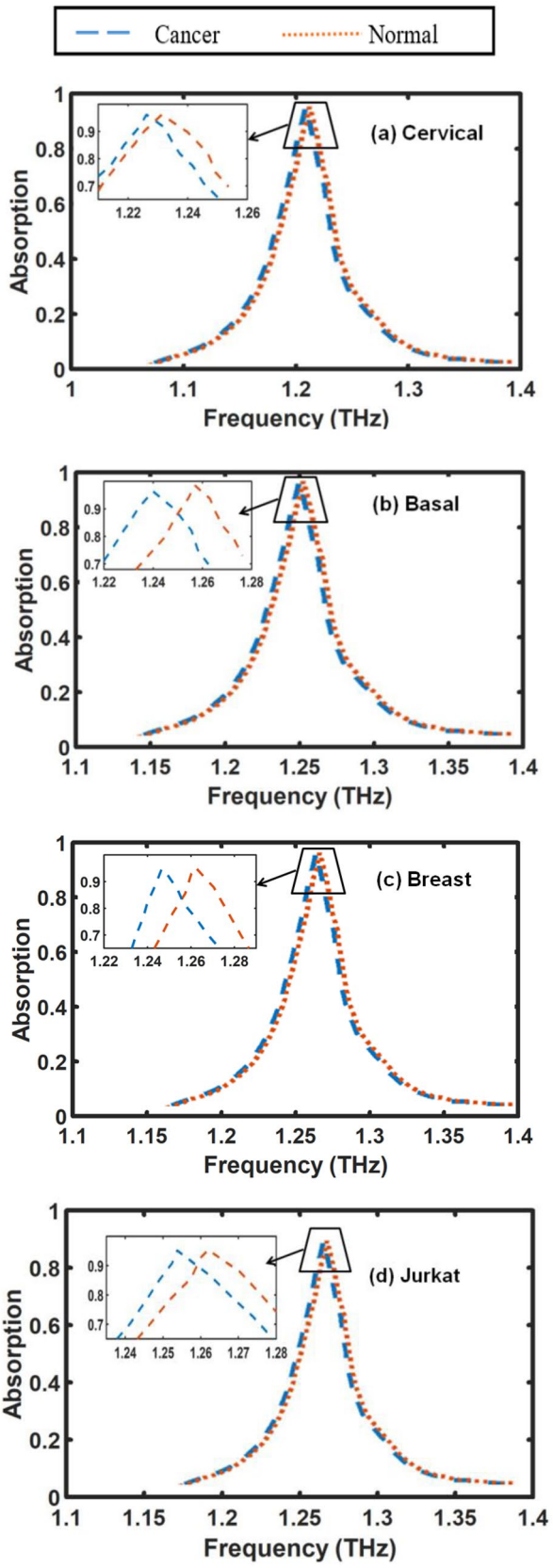

Fig. 12 The absorption spectrum of the metamaterial biosensor using different normal and cancerous cells

Table 2 The average sensitivity of the reported biosensor compared to the recent biosensors

Research	Sensing Application	Sensor Sensitivity GHz/RIU
Ref [36]	breast,cervical cancer, colorectal cancer	207.14
Ref [32]	Cervical cancer	74
Ref [48]	Lung cancer and brain cancer	504
Ref [49]	Breast cancer detection	325
Ref [50]	Detection of Brain Tumor	153.85
Ref [34]	vivo-like cells	287
Ref [22]	Breast cancer, skin cancer	488
Ref [40]	Breast cancer, Blood cancer	495
Ref [51]	liver cancer	150
Ref [52]	Liver Cancer detection	642.5
Current work	Cancer detection of basal cell, breast cell, Jurkat cell and Cervical cell	556.325

coating, and the patterns will be converted from photomasks to photoresists through UV irradiation and will be developed within the framework of AZ300 MIR. Photolithography can also be used to obtain metallic patches.

Conclusion

We proposed and analyzed novel metamaterial biosensor for Hb concentration detection and for early cancer detection with high sensitivity. Full vectorial finite element method is used to simulate the studied designs. The reported biosensor can detect the analyte refractive index change with high linear sensitivity. High sensor sensitivity of 1.08 GHz/g/dL is achieved at 1.1 THz with a narrow resonant peak and high Q-factor of 13.2 for Hb concentration detection. Further, an average sensitivity of 556.325 GHz/RIU is achieved for cancer early detection for basal cell, breast cell, Jurkat cell and Cervical cell which is greater than those presented in the literature with simple design. Moreover, the proposed sensor can be fabricated using current technologies that have already been employed in the fabrication of similar designs.

Author Contributions Mohamed Farhat O. Hameed proposed the idea. Mahmoud Maree. E. Tammam have made the simulation results and wrote the first draft. All authors have contributed to the analysis, discussion, writing and revision of the paper.

Funding Open access funding provided by The Science, Technology & Innovation Funding Authority (STDF) in cooperation with The Egyptian Knowledge Bank (EKB). The authors acknowledge the financial support from the Science, Technology & Innovation Funding Authority (STIFA) in Egypt under the project (ID: 45702).

Data Availability No datasets were generated or analysed during the current study.

Declarations

Ethical Approval The authors declare that there are no conflicts of interest related to this article.

Competing Interests The authors declare no competing interests.

References

1. Chen T, Li S, Sun H (2012) Metamaterials Application in Sensing. Sensors 12(3):2742–2765
2. Smith DR, Padilla WJ, Vier DC, Nemat-Nasser SC, Schultz S (2000) Composite medium with simultaneously negative permeability and permittivity. Phys Rev Lett 84(18):4184–4187. https://doi.org/10.1103/PhysRevLett.84.4184. PMID: 10990641
3. Engheta N, Ziolkowski RW (2006) Metamaterials: Physics and Engineering Explorations. IEEE Press, The Institute of Electrical and Electronics Engineers Inc
4. Eleftheriades GV, Balmain KG (2005) Negative Refraction Metamaterials: Fundamental Principles and Applications, 1st edn. John Wiley & Sons, Hoboken
5. Bruen D, Delaney C, Florea L, Diamond D (2017) Glucose Sensing for Diabetes Monitoring: Recent Developments. Sensors (Basel, Switzerland) 17
6. Karaaslan M, Bakir M (2014) Chiral Metamaterial Based Multifunctional Sensor Applications. Progress In Electromagnetics Research 149:55–67
7. Tao Hu, Landy NI, Bingham CM, Zhang X, Averitt RD, Padilla WJ (2008) A metamaterial absorber for the terahertz regime: Design, fabrication and characterization. Opt Express 16:7181–7188
8. Bağmancı M, Karaaslan M, Unal E, Akgol O, Sabah C (2017) Extremely-broad band metamaterial absorber for solar energy harvesting based on star shaped resonator. Opt Quantum Electron 49. https://doi.org/10.1007/s11082-017-1091-7
9. Yang J, Huang M, Yang C, Xiao Z, Peng J (2009) Metamaterial electromagnetic concentrators with arbitrary geometries. Opt Express 17:19656–19661
10. Dincer F, Akgol O, Karaaslan M, Unal E, Sabah C (2014) Polarization Angle Independent Perfect Metamaterial Absorbers for Solar Cell Applications in the Microwave, Infrared, and Visible Regime. Prog Electromagn Res 144:93–101. https://doi.org/10.2528/PIER13111404
11. Pendry JB (2000) Negative Refraction Makes a Perfect Lens. Phys Rev Lett 85:3966–3969. https://doi.org/10.1103/PhysRevLett.85.3966

12. Ghanim A, Hussein M, Hameed MFO, Yahia AS, Obayya S (2016) Highly directive hybrid Yagi-Uda nanoantenna for directional emission enhancement. IEEE Photonics J 1–1. https://doi.org/10.1109/JPHOT.2016.2615596
13. Tao Hu, Bingham C, Strikwerda A, Pilon D, Shrekenhamer D, Landy N, Fan K, Zhang X, Padilla W, Averitt R (2008) Highly flexible wide angle of incidence terahertz metamaterial absorber: Design, fabrication, and characterization. Phys Rev B 78:241103(R). https://doi.org/10.1103/PhysRevB.78.241103
14. Areed NF, Zienab EW, Obayya SSA (2018) Nearly perfect metamaterial plasmonic absorbers for solar energy applications. Opt Quant Electron 50(4):197
15. Schüßler M, Mandel C, Puentes M, Jakoby R (2012) Metamaterial Inspired Microwave Sensors. IEEE Microwave Magazine - IEEE MICROW MAG 13:57–68. https://doi.org/10.1109/MMM.2011.2181448
16. Lee H-J, Yook J-G (2008) Biosensing using split-ring resonator at microwave regime. Appl Phys Lett 92:254103–254103. https://doi.org/10.1063/1.2946656
17. Huang M, Yang J (2011) Microwave Sensor Using Metamaterials. https://doi.org/10.5772/14459
18. Samy A, Hameed MFO, Elkaramany E, Obayya S (2019) Highly Sensitive Terahertz Metamaterial Sensor. IEEE Sens J 1–1. https://doi.org/10.1109/JSEN.2019.2918214
19. Park S, Cha S, Shin G, Ahn Y (2017) Sensing viruses using terahertz nano-gap metamaterials. Biomed Opt Express 8:3551–3558. https://doi.org/10.1364/BOE.8.003551
20. Park S, Hong JT, Jin CS, Kim H-S, Park W-K, Han S, Park J, Lee S, Kim D-S, Ahn Y (2014) Detection of microorganisms using terahertz metamaterials. Sci Rep 4:4988. https://doi.org/10.1038/srep04988
21. Haq T, Ruan C, Zhang X, Ullah S (2019) Complementary Metamaterial Sensor for Nondestructive Evaluation of Dielectric Substrates. Sensors 19:2100. https://doi.org/10.3390/s19092100
22. Zhang H, Liu C, Xu C, Li Z, Wang Y, Peng Y (2023) A dual-band terahertz metamaterial sensor with high Q-factor and sensitivity. Opt Quantum Electron 55. https://doi.org/10.1007/s11082-023-05456-7
23. Baqir A, Choudhury P (2022) Hyperbolic Metamaterial-Based Optical Biosensor for Detecting Cancer Cells. IEEE Photonics Technol Lett 1–1. https://doi.org/10.1109/LPT.2022.3228943
24. Akhdar H, Nataraj SK, Alinad T, Sivanesan T, Alanazi N, Alodhayb A (2023) Blood component detection using photonic crystal fibre sensor. Opt Quantum Electron 56. https://doi.org/10.1007/s11082-023-05621-y
25. Olyaee S, Seifouri M, Mohsenirad H (2016) Label-free detection of glycated haemoglobin in human blood using silicon-based photonic crystal nanocavity biosensor'. J Mod Opt 63(13):1274–1279
26. Ibrahim MSS, Tarek M, Obayya SSA, Hameed MFO (2021) Highly Sensitive 1D Photonic Crystal Biosensor. 2021 International Applied Computational Electromagnetics Society Symposium (ACES), Hamilton, ON, Canada pp 1–2
27. Kiroriwal M, Singal P, Sharma M, Singal A (2022) Hemoglobin sensor based on external gold-coated photonic crystal fiber. Opt Laser Technol 149:107817 ISSN 0030–3992
28. El-Khozondar H, Mahalakshmi P, El-Khozondra R, Ramanujam N, Amiri IS, Yupapin P (2019) Design of one dimensional refractive index sensor using ternary photonic crystal waveguide for plasma blood samples applications. Physica E: Low Dimens Syst Nanostruct 111. https://doi.org/10.1016/j.physe.2019.02.030
29. Doshi R, Panditrao AM (2013) Optical Sensor System for Hemoglobin Measurement
30. Timm U, Mcgrath D, Lewis E, Kraitl J, Ewald H (2009) Sensor System for Non-Invasive Optical Hemoglobin Determination. Proceedings of IEEE Sensors 1975 - 1978. https://doi.org/10.1109/ICSENS.2009.5398321
31. Cong L, Singh R (2014) Sensing with THz metamaterial absorbers. arXiv preprint arXiv:1408.3711
32. Li D et al (2021) Identification of early-stage cervical cancer tissue using metamaterial terahertz biosensor with two resonant absorption frequencies. IEEE J Sel Top Quantum Electron 27(4):8600107. https://doi.org/10.1109/JSTQE.2021.3058163
33. Zhang Z, Ding H, Yan X, Liang L, Wei D, Wang M, Yang Q, Yao J (2018) Sensitive Detection of Cancer Cell Apoptosis Based on the Non-Bianisotropic Metamaterials Biosensors in Terahertz Frequency. Opt Mater Express 8:659
34. Han L, Wang Y, Chen K, Gao H, Xia K, Ge Q, Yang J, Shi W, Ruan C (2024) Detection of In Vivo-Like Cells by a Biosensor Chip Based on Metamaterials in Terahertz Regime. Biosensors 14:230. https://doi.org/10.3390/bios14050230
35. Manikandan E, Karthigeyan KA, Arivarasi A, Papanasam E (2023) High-Q and FOM dual-band polarization dependent ultra-narrowband terahertz metamaterial sensor. IEEE Photonics J 15(1):0600206. https://doi.org/10.1109/JPHOT.2023.3234074
36. Patel SK, Surve J, Parmar J (2022) Detection of cancer with graphenemetasurface-based highly efficient sensors. Diamond Related Mater 129:109367. https://doi.org/10.1016/j.diamond.2022.109367
37. Sabah C, Mulla B, Altan H, Ozyuzer L (2018) Cross-like terahertz metamaterial absorber for sensing applications. Pramana 91. https://doi.org/10.1007/s12043-018-1591-4
38. Assal A, Breiss H, Benzerga R, Jrad A, Harmouch A (2020) Toward an Ultra-Wideband Hybrid Metamaterial Based Microwave Absorber. Micromachines 11. https://doi.org/10.3390/mi11100930
39. Abdulkarim YI et al (2022) Highly Sensitive Dual-Band Terahertz Metamaterial Absorber for Biomedical Applications: Simulation and Experiment. ACS omega 7(42):38094–38104. https://doi.org/10.1021/acsomega.2c06118
40. Mezache Z, Hafdi Z, Tao J (2023) Design of a novel graphene buzzle metamaterial refractometer for sensing of cancerous cells in the terahertz regime. Optik 287:171170. https://doi.org/10.1016/j.ijleo.2023.171170
41. Zhan Y, Yin H, Wang J, Yao H, Fan C (2022) Tunable multiple band THz perfect absorber with InSb metamaterial for enhanced sensing application. Results in Optics 8:100255. https://doi.org/10.1016/j.rio.2022.100255
42. Tao Hu, Strikwerda A, Liu M, Mondia J, Ekmekci E, Fan K, Kaplan D, Padilla W, Zhang X, Averitt R, Omenetto F (2010) Performance enhancement of terahertz metamaterials on ultrathin substrates for sensing applications. Appl Phys Lett 97:261909. https://doi.org/10.1063/1.3533367
43. Wang J, Lang T, Hong Z, Xiao M, Yu J (2021) Design and Fabrication of a Triple-Band Terahertz Metamaterial Absorber. Nanomaterials 11:1110
44. COMSOL Multiphysics http://www.comsol.com
45. Bashkatov AN, Genina EA (2003) Water refractive index in dependence on temperature and wavelength: a simple approximation. Proceedings of SPIE 5068, Saratov Fall Meeting 2002: Optical Technologies in Biophysics and Medicine IV
46. Friebel M, Meinke M (2006) Model function to calculate the refractive index of native hemoglobin in the wavelength range of 250–1100 nm dependent on concentration. Appl Opt 45:2838–2842. https://doi.org/10.1364/AO.45.002838
47. Azab MY, Hameed MFO, Nasr AM, Obayya SSA (2021) Highly sensitive metamaterial biosensor for cancer early detection. IEEE Sensors J 21(6):7748–7755. https://doi.org/10.1109/JSEN.2021.3051075
48. Wang P, Lou J, Yu Y et al (2023) An ultra-sensitive metasurface biosensor for instant cancer detection based on terahertz spectra. Nano Res 16:7304–7311. https://doi.org/10.1007/s12274-023-5386-7

49. Fang W, Ma Z, Lv X, Liu J, Pei W, Geng Z (2022) Flexible terahertz metamaterial biosensor for label-free sensing of serum tumor marker modified on a non-metal area. Opt Express 30:16630–16643
50. Alsalman O, Wekalao J, Arunkumar U, Agravat D, Parmar J, Patel SK (2023) Design of Split Ring Resonator Graphene Metasurface Sensor for Efficient Detection of Brain Tumor. Plasmonics 19. https://doi.org/10.1007/s11468-023-02002-9
51. Geng Z, Zhang X, Fan Z, Lv X, Chen H (2017) A Route to Terahertz Metamaterial Biosensor Integrated with Microfluidics for Liver Cancer Biomarker Testing in Early Stage. Sci Rep 7(1):16378. https://doi.org/10.1038/s41598-017-16762-y.PMID:29180650;PMCID:PMC5704020
52. Li Z (2023) Split ring multiband refractive index cancer sensor based on terahertz radiation. Appl Opt 62:8558–8566
53. Ling K, Yoo M, Kim K, Lim S, Su W, Cook B, Tentzeris M (2015) Microfluidically tunable paper-based inkjet-printed metamaterial absorber. 218–220. https://doi.org/10.1109/IWAT.2015.7365331